

International Conference on Space Optics—ICSO 2018

Chania, Greece

9–12 October 2018

Edited by Zoran Sodnik, Nikos Karafolas, and Bruno Cugny



Radiation tests on the COTS image sensor from CMOSIS

Pawel Adamiec

Juan Barbero

Alejandro Lopez Moya

Enrique Cordero



Radiation tests on the COTS image sensor from CMOSIS

Pawel Adamiec, Juan Barbero, Alejandro Lopez Moya, Enrique Cordero
ALTER TECHNOLOGY TÜV NORD S.A.U., C/ la Majada 3, 28760 Tres Cantos, Spain

ABSTRACT

12 Mpix color commercial-of-the-shelf (COTS) image sensor from CMOSIS was tested with proton radiation. The target mission required an irradiation with protons of energy of 50 MeV and fluences up to $1 \cdot 10^{12}$ p/cm². Several intermediate steps were introduced to check the behavior of the image sensor. A low-cost test camera was developed to control the image sensors, acquire the images, and monitor the currents and voltages during the tests. Each color was characterized separately according to the EMVA 1288 standard. Such treatment allowed also analysis of the bayer filter deposited on the image sensor surface. Post-radiation characterization revealed that a significant deterioration in the parameter performance was found independently of the pixel color. The most affected parameters were dark current and dark signal nonuniformities (DSNU) which have increased from about one to two orders of magnitude.

Keywords: Image sensor, CMOS, CIS, dark current, DSNU, proton radiation, displacement damage, NIEL

1. INTRODUCTION

In the last years the complementary metal-oxide-semiconductor (CMOS) active pixel sensors (APS) have overcome several technological problems and are competing with their counterparts, namely: coupled-charged devices (CCD) [1-4]. They were successfully used in several space missions ie. IRIS1 in XMM or Cluster II missions in on-board cameras for visual feedback of spacecraft-launcher separation or antenna deployment [5], HAS in PROBA-2 mission for solar observations [6], Cobra in COMS-1 for ocean color imaging [7], or Sapphire in UKube-1 [8]. Although the radiation hard devices are available as custom design and they were widely investigated in harsh environment [9-13] it is worth to mention that even commercial-off-the-shelf (COTS) CMOS image sensors (CIS) are of interest for space applications [8] due to their low cost and availability. This trend is becoming stronger in the recent years and nowadays the COTS components are tested considering mission parameters as orbit, duration, spacecraft shielding, etc. Thus, reducing substantially costs and time necessary for design and manufacturing of a rad-hard components and the overall mission costs eventually.

Every CIS is characterized by set of parameters which usually deteriorate during radiation tests, but in the majority cases the most affected parameter is the dark current [9]. It is a primary source of noise in an imager due to lattice defects or metal impurities in the silicon lattice of the image sensor [14]. A lattice defect or impurity creates an alternative current path and therefore they can be collected in depletion region, partially filling the potential well. Dark current is a main problem in a low-light photography where the dark current competes with the current generated by the incident light which is the case of the space cameras. Additionally, dark current varies from pixel to pixel on the image sensor due to variations in defects and impurities creating the largest source of dark signal nonuniformities (DSNU) and fixed pattern noise (FPN). Since the dark current depends strongly on the number of defects it is the proton radiation which should deteriorate substantially the performance of the image sensor because it is responsible for displacement damage in the material (defects creation). Additionally, protons are the important radiation source in the low earth orbit (LEO). Therefore, in this paper we present the results of the proton radiation tests on the COTS CIS from CMOSIS (CMV12000) with the fluences up to 10^{12} p/cm². The image sensor will be used in the LEO mission.

2. EXPERIMENTAL

2.1 Sample description

CMV12000 image sensor consists of about 12 Mpix organized in an array of 3072 x 4096 pipelined global shutter pixels which allow exposure during read-out. The size of the pixel is 5.5 μ m x 5.5 μ m. There are 5 supply voltages: VDD33 = 1.98 V, VDD33 = 3.3 V, VDD_PIX = 3 V, VDD_RES = 3.3 V, and VDD18_PLL = 1.98 V. The image sensor has 64 8-, 10- or 12-bit digital low-voltage differential-signaling (LVDS) outputs (serial). The image sensor also integrates a

programmable gain amplifier and offset regulation. It can be programmable using the serial peripheral interface (SPI). In our experiment 16 LVDS lanes at 10 bits were used. Since it is the color image sensor it has an RGB bayer filter deposited on the surface of the pixels. The sequence is shown in Figure 1. The letters indicate the colors GB – green pixel in the row with blue pixels, B – blue, R – red, GR – green pixel in the row with red pixels.

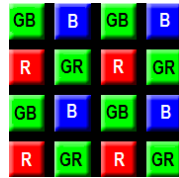


Figure 1. Color sequence in the bayer filter for CMV12000 image sensor.

2.2 Test camera and electrical setup

The camera is an elegant breadboard which allows reading the images, driving the image sensor with internal or external sources, and reading/writing the registers (see Figure 2). It consists of three main parts: (i) a motherboard with the necessary electronics to communicate with the image sensor like FPGA, memory, UDP for image transfer and RS 232 to access the registers, (ii) LVDS bridge for CMV12000 which allows driving the imager with external sources and monitor the supply voltages and currents, (iii) a small remote PCB with the zero-insertion socket to hold the imager with accompanying decoupling passive elements. The remote PCB is connected to LVDS bridge by means of 4 HDMI cables, making the camera flexible for different radiation setups as well as for temperature/vacuum setups. This camera is working with 200 MHz clock and the image transfer is up to 1 Gbit/s. Since the FPGA can be programmed for different image sensors and only the small PCB needs to be changed for another image sensor, this solution is very cheap and let to save a lot of development time.

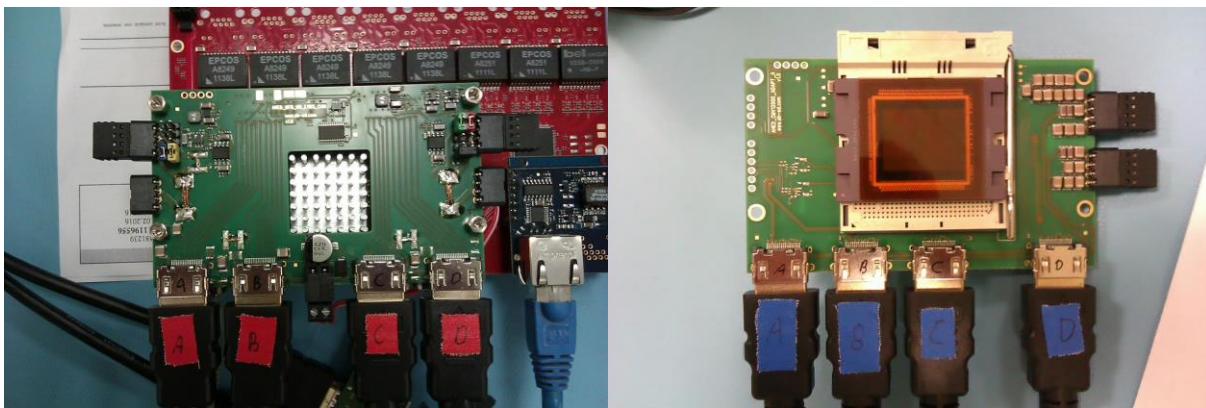


Figure 2. Left: picture of the LVDS bridge plugged to the motherboard. Right: Remote PCB with image sensor.

The image sensor was driven by means of two Keithley 2230G-30-1 power supplies and the currents and voltages were monitored by means of Data Acquisition Unit Agilent 34970A. The values of voltages were set as indicated in the section 2.1 in all five supply rails.

To check the integrity of the internal electronics also the built-in pattern was read during initial, intermediate, and final measurements.

2.3 Optical setup

The optical measurements were made according to EMVA Standard 1288 – Standard for Characterization of Image Sensor and Cameras, Release 3.0, November 29, 2010. Since CMV12000 is an RGB color image sensor, it is necessary to characterize each pixel color separately. Therefore, the optical setup consists of a color light source (three LEDs: red, green, and blue), integrating sphere (Newport 819-SF-6), power meter (Newport 2936-C) with photodetector (Newport 883-SL), wavelength meter (Thorlabs CCS200). The linearity of the light source is better than 0.995 measured from the center of the image sensor to the edges. The scheme is shown in the Figure 3.

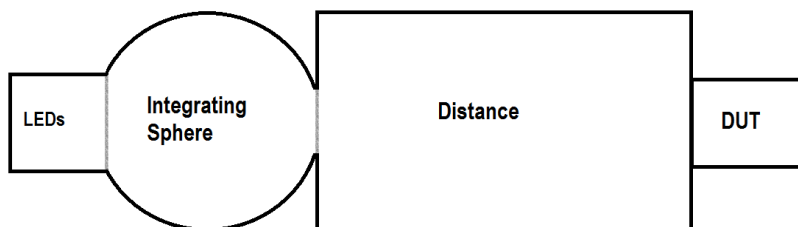


Figure 3. Schematic of the optical setup.

The distance between the output of the integrating sphere to the DUT is set to 8 times the aperture of the integrating sphere. The device under test (DUT) was replaced with power meter as well as wavelength meter to measure the properties of incident light. The power and wavelengths were as follows: red – 630 nm – 69 nW; green – 535 nm – 70 nW; blue – 465 nm – 69 nW. The full width at half maximum (FWHM) < 50 nm for each color. The values of the power were set to allow relatively long exposure times before saturation of the images. The exposure times for photon transfer method (PTM) were in the range from 1 ms to 600 ms. Two dark and two gray (flat) images were taken at each exposure time. For DSNU and photo response nonuniformity (PRNU) the images were taken at exposure time corresponding to 50% of the full well saturation. The images for dark current calculations were taken at 6 equally spaced exposure times from 100 ms to 600 ms.

2.4 Proton radiation setup

Experiments with high energy protons of 50 MeV were conducted at Université catholique de Louvain (UCL), Belgium. At UCL a CYCLONE110 (CYClotron de LOuvain-la-NEuve) is a multiparticle, variable energy, isochronous cyclotron capable of accelerating protons up to 65 MeV. The beam diameter was of about 90 mm and the flux can be adjusted to the needs of the applications. For this mission the necessary safe fluence for the spacecraft was estimated at the level of 10^{11} p/cm². Therefore, the final fluence was chosen as 10 times the safe fluence. The intermediate steps and the radiation conditions are listed in the Table 1. The image sensor was non-operational during the irradiation and only dark current measurements were performed as the intermediate measurements. During irradiation the image sensor was placed in similar board as remote PCB, but all the rails were short-circuited.

Table 1. Radiation conditions

| | Unit | Step 1 | Step 2 | Step 3 | Step 4 |
|---------------|----------------------|--------|--------|--------|--------|
| Proton energy | MeV | 50 | 50 | 50 | 50 |
| Fluence | p/cm ² | 1e+9 | 1e+10 | 1e+11 | 1e+12 |
| Flux | p/cm ² /s | 1e+7 | 1e+8 | 1e+8 | 1e+8 |
| Exposure time | min | 1.7 | 1.7 | 16.7 | 160 |

3. RESULTS AND DISCUSSION

Characterization consists of several points: (i) acquiring of the set of images with different exposure times for PTM, dark current, and DSNU/PRNU, (ii) acquisition of internal test pattern, (iii) monitoring of currents and voltages. The PTM was performed only for the pristine devices and as final measurements at ALTER labs. The final measurement was taken about one week after the irradiation because the samples were activated and had to remain in the radiation facility. Dark current was measured during the intermediate steps at the radiation facility. All the measurements and radiation tests were performed at room temperature 22 ± 3 °C.

Monitoring of currents and voltages was performed during image acquisition. The voltage values were constant during all the operation time of the image sensor and read; VDD18 – 1.98 V, VDD18_PLL – 1.98 V, VDD33 – 3.296 V, VDD_RES – 3.3 V, VDD_PIX – 2.999 V. The currents showed negligible changes (see Figure 4) except VDD_PIX which is a peak current which occurs for some ms during image acquisition up to 1 A. Since the monitoring is much slower and not synchronized with image acquisition such changes can be observed when the image sensor is switching between standby and acquisition mode.

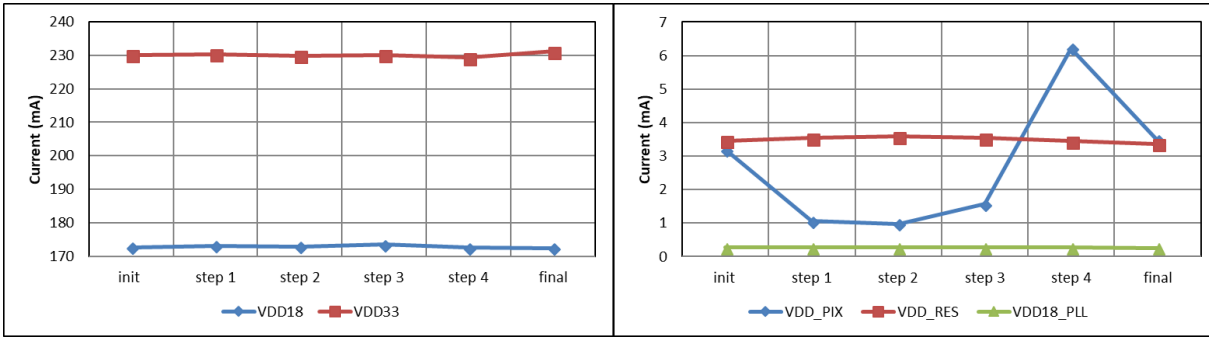


Figure 4. Evolution of the supply currents at different radiation steps.

Pixel performance obtained by PTM is shown in the Table 2. The letter ‘i’ means the initial value and letter ‘f’ the value after final measurements. In general, all the parameters showed strong deterioration after receiving the fluence of $1 \cdot 10^{12}$ p/cm² but some of them behave differently depending of the pixel color. Blue and red pixels showed 50% decrease in the responsivity, whereas the green pixels of about 30%. Similar trend, showing that the performance of blue and red pixels is worse than green pixels is seen also for quantum efficiency, saturation capacity, and linearity error. The dynamic range and signal to noise ratio decreased up to 50% and 25%, respectively. In this case, however, all the colors behave in the same way. The increase of the linearity error indicates that the deviation of the measured characteristics from the ideal one has increased.

Table 2. Pixel performance. SNR – signal to noise ratio

| Sample number | Responsivity | Quantum efficiency | Saturation capacity | Dynamic range | Temporal dark noise | Linearity error | SNR _{max} |
|---------------|--------------|--------------------|---------------------|---------------|---------------------|-----------------|--------------------|
| | A/W | % | e- | dB | e- | % | dB |
| 218 GB i | 0.15 | 35 | 6492 | 39 | 68 | 0.93 | 38.1 |
| 218 GB f | 0.10 | 23 | 2018 | 22 | 98 | 2.04 | 33.0 |
| 218 GR i | 0.16 | 37 | 7828 | 42 | 64 | 0.92 | 38.9 |
| 218 GR f | 0.10 | 22 | 2296 | 22 | 90 | 2.10 | 32.9 |
| 218 B i | 0.15 | 39 | 7473 | 40 | 69 | 0.99 | 38.7 |
| 218 B f | 0.06 | 17 | 1222 | 21 | 67 | 2.44 | 30.9 |
| 218 R i | 0.18 | 35 | 7459 | 41 | 65 | 0.95 | 38.7 |
| 218 R f | 0.08 | 16 | 1079 | 21 | 55 | 2.62 | 30.3 |

The mean dark current, the DSNU and PRNU are shown in the Table 3. The mean dark current was determined by averaging the dark signal of all the pixels with the same color at each exposure time. After the irradiation the PRNU increased twice and DSNU increased about 5 times irrespective of the pixel color. In the case of the dark current the increase is about two orders of magnitude.

Table 3. Dark currents, PRNU, and DSNU – initial and final measurements.

| Sample number | | 218 GB i | 218 GB f | 218 GR i | 218 GR f | 218 B i | 218 B f | 218 R i | 218 R f |
|---------------|-------------------|----------|----------|----------|----------|---------|---------|---------|---------|
| Dark current | DN/s | 6.86 | 650 | 6.79 | 650 | 6.86 | 645 | 6.79 | 650 |
| | e ⁻ /s | 56.2 | 5220 | 58.2 | 5498 | 56.7 | 5264 | 59.0 | 5561 |
| PRNU | % | 1.62 | 3.13 | 1.61 | 3.15 | 1.64 | 3.5 | 1.52 | 2.83 |
| DSNU | DN | 1.92 | 9.27 | 1.92 | 9.28 | 1.92 | 9.29 | 1.91 | 9.27 |

The evolution of the dark current is shown in the Figure 5. The increase in the dark current is expected due to displacement damage and ionization effects and it is comparable with other results for CIS irradiated with 50 MeV

protons [15]. The experimental generation lifetime damage factor K [16, 17] was calculated as the slopes of the lines in Figure 5 (right). The values of K for different colors for 50 MeV protons read: $K_{GB} = 3.36 \cdot 10^{-12}$, $K_{GR} = 3.57 \cdot 10^{-12}$, $K_B = 3.39 \cdot 10^{-12}$, and $K_R = 3.6 \cdot 10^{-12}$ all in units of nA/particle. The values are slightly different between the different colors but are in line with other values reported for 50 MeV protons in silicon [18]. The decrease observed in the final measurement is the effect of the annealing processes since the measurement was taken one week after the irradiation campaign (room temperature storage). As explained in [18] these processes can be divided into two types: (i) induced defects experience a fast recovery after the irradiation due to the recombination and rearrangement of defects; (ii) permanent damage which is a damage remaining after completion of the short-term anneal. Indeed, a long-term annealing is still observed with very slow annealing rates. In our case, after annealing of about 170 hours at room temperature the devices have recovered of about 26% irrespective of the pixel color concerning dark current.

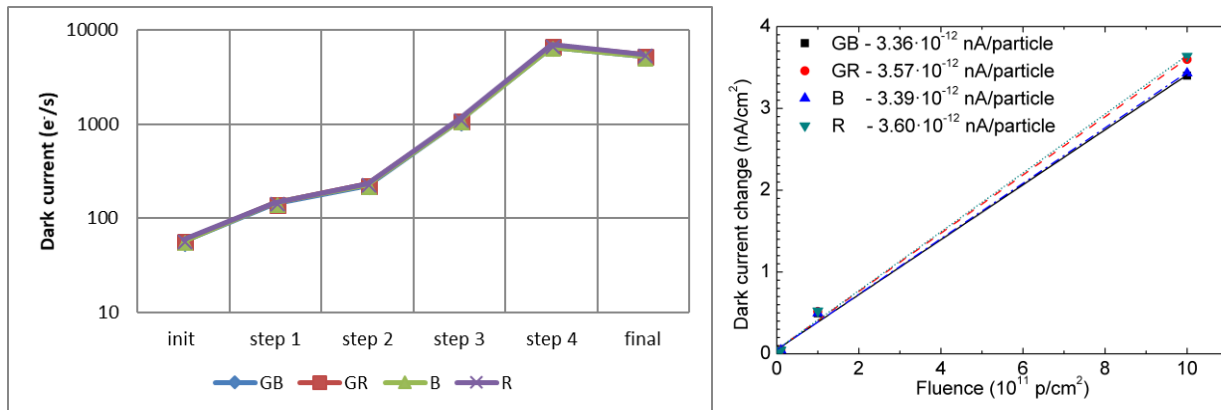


Figure 5. Left: Evolution of the dark current during radiation test. The steps correspond to the fluences: $1e+9$, $1e+10$, $1e+11$, and $1e+12$ p/cm² starting from step 1 to step 4. Right: Dark current change dependence on the fluence for all pixel colors.

In the Figure 6 histograms of the dark signal are shown for different exposure times after irradiation with fluence $1 \cdot 10^{11}$ p/cm² and evolution of the dark signal after different irradiation steps at 200 ms (initial exposure time for 50% of saturation capacity) for GB pixels. Analyzing the dark signal histograms allows to find rapidly defect pixels in the pristine devices and the evolution of the imager response to different external perturbations like temperature change, radiation, etc. In the case of the studied CIS, the pristine device showed one hot pixel (completely saturated) in green-blue set of pixels. Besides, the image sensor response was quite homogenous, about 0.1% and 1.5% of the pixels could be considered as outliers or deviated from the gaussian fit to the logarithmic histogram [19] for 100 ms and 600 ms, respectively. After irradiation with 10^{11} p/cm² the number of outliers and hot pixels increased significantly. The number of hot pixels reached about 10^5 in comparison to only 1 for the pristine device at 600 ms exposure time. At the right-hand side of Figure 6, it can be seen, that with increasing fluence more pixels differ from the gaussian form of the histogram. For the fluence of $1 \cdot 10^{12}$ p/cm² the deviation is about 20% of the overall pixel number for exposure time of 200 ms. This is very important information for space application where the integration time can be quite large.

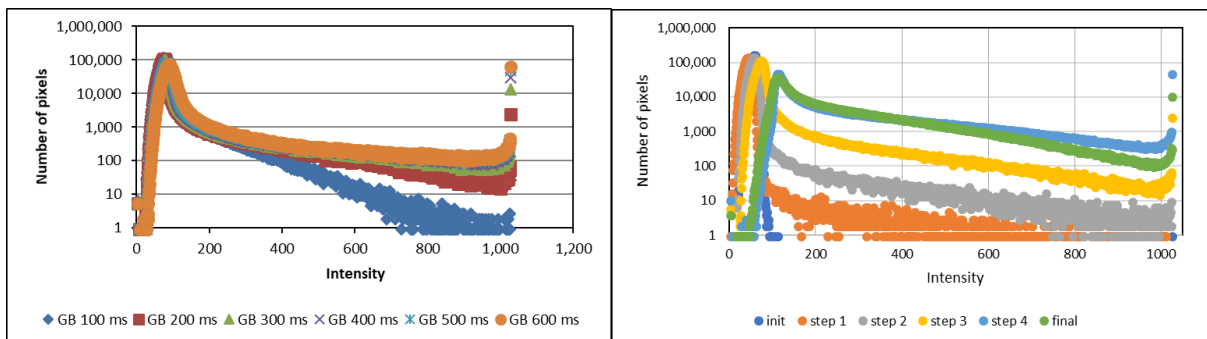


Figure 6. Left: Logarithmic dark signal histogram after irradiation with fluence of $1 \cdot 10^{11}$ p/cm² at different exposure times. Right: Logarithmic dark signal histogram at 200 ms exposure time for different irradiation steps.

To have complete image of the dark current changes, a histogram of dark currents of each pixel is shown in Figure 7. At the left-hand side there is a histogram for four pixel colors after the irradiation with fluence of $1 \cdot 10^{11}$ p/cm². The mean value of dark current for all color pixels is about 1000 e⁻/s, which is also seen in the histogram. The right-hand side of the Figure 7 shows a logarithmic histogram of dark current for green-blue pixels for different irradiation steps. It is interesting that this sensor shows well known exponential tail in the dark current histogram for pristine device and for lowest fluence of $1 \cdot 10^9$ p/cm² [9]. For the higher fluences a second peak between 14 – 16 ke⁻/s can be observed, and it is more pronounced for fluence $1 \cdot 10^{12}$ p/cm². Similar second peak was observed by Beaumel in HAS2 imager after irradiation with 62 MeV protons with fluence of $1.95 \cdot 10^{11}$ p/cm² [20]. After the second peak an exponential tail can be seen.

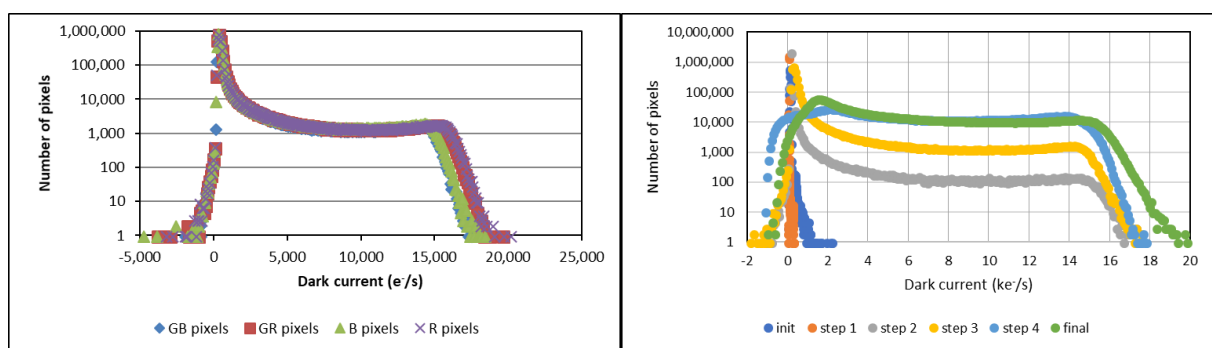


Figure 7. Left: Logarithmic dark current histogram after irradiation with fluence of $1 \cdot 10^{11}$ p/cm². Right: Logarithmic dark current histogram for GB pixel at different irradiation steps.

4. SUMMARY AND CONCLUSIONS

Radiation test with 50 MeV protons have been performed on COTS CMV12000 image sensor from CMOSIS. After irradiation to final fluence of $1 \cdot 10^{12}$ p/cm² and one week of annealing the image sensor showed a strong degradation of performance. Although all pixel colors were affected, the most susceptible for proton radiation were blue and red pixels, which is especially visible in the responsivity, quantum efficiency, and saturation capacity. Since the entire image sensor is made of the same material (Si) it is the bayer filter composition for red and blue pixels which has affected those parameters. The DSNU and dark current increased about 5 and 100 times, respectively, independently of the color pixel. Thus, confirming that it is bayer filter which affects the measurements which required illumination with light.

We have developed an EMVA standard compliant system for characterizing image sensors and developed a low-cost camera to drive different types of image sensor. The camera consists of the main electronics and the remote socket to hold an image sensor, which makes it flexible test board for temperature, vacuum or radiation tests with image sensors.

REFERENCES

- [1] Janesick, J., Andrews, J. T., and Elliot, T., “Fundamental performance differences between CMOS and CCD imagers; Part I,” Proc. SPIE 6276, 6276M (2006).
- [2] Janesick, J., Andrews, J., Tower, J., Grygon, M., Elliot, T., Cheng, J., Lesser, M., and Pinter, J., “Fundamental performance differences between CMOS and CCD imagers; Part II,” Proc. SPIE 6690, 669003 (2007).
- [3] Magnan, P., “Detection of visible photons in CCD and CMOS: A comparative review,” Nucl. Instr. Meth. Phys. Res. A 504, 199-212 (2007).
- [4] Fossum, E.R., and Hondongwa, D.B., “A review of the pinned photodiode for CCD and CMOS image sensors,” IEEE J. Electron Devices Soc. 2, 33-43 (2014).
- [5] Habinc, S., Karlsson, A., Wijmans, W., Jameux, D., Ogiers, W., and de Vos, L., “In-flight results using visual monitoring cameras,” Proc. DASIA, 71-76 (2000).
- [6] De Groof, A., Berghmans, D., Nicula, B., Halain, J-P., Defise, J-M., Thibert, T., and Schühle, U., “CMOS-APS detectors for solar physics: lessons learned during the SWAP preflight calibration,” Solar Phys. 249, 147-163 (2008).

- [7] Wang, M., Ahn, J-H., Jiang, L., Shi, W., Son, S. H., Park, Y-J., and Ryu, J-H., "Ocean color products from Korean Geostationary Ocean Color Imager (GOCI)," *Opt. Express* 21, 3835-3849 (2013).
- [8] Harriss, R. D., Holland, A. D., Barber, S. J., Karout, S., Burgon, R., Dryer, B. J., Murray, N. J., Hall, D. J., Smith, P. H., Grieg, T., Tutt, J. H., Endicott, J., Jerram, P., Morris, D., Robbins, M., Prevost, V., and Holland, K., "Compact CMOS Camera Demonstrator (C3D) for Ukube-1", *Proc. SPIE* 8146, 81460U (2011).
- [9] Bogaerts, J., Dierickx, B., Meynants, G., and Uwaerts, D., "Total dose and displacement damage effects in a radiation-hardened CMOS APS," *IEEE Trans. Electron Devices* 50, 84–90 (2003).
- [10] Beaumel, M., Herve, D., Van Aken, D., Pourrouquet, P., and Poizat, M., "Proton, electron, and heavy ion single event effects on the HAS2 CMOS image sensor," *IEEE Trans. Nucl. Sci.* 61, 1909-1917 (2014).
- [11] Eid, E-S., Chan, T. Y., Fossum, E. R., Tsai, R. H., Spagnuolo, R., Deily, J., Byers, W. B., and Peden, J. C., "Design and characterization of ionizing radiation-tolerant CMOS APS image sensor up to 30 Mrd (Si) total dose," *IEEE Trans. Nucl. Sci.* 48, 1796-1806 (2001).
- [12] Goiffon, V., Corbiere, F., Rolando, S., Estriebeau, M., Magnan, P., Avon, B., Baer, J., Gaillardin, M., Molina, R., Paillet, P., Girard, S., Chabane, A., Cervantes, P., and Marcandella, C., "Multi-MGy Radiation Hard CMOS Image Sensor: Design, Characterization and X/Gamma Rays Total Ionizing Dose Tests," *IEEE Trans. Nucl. Sci.* 62, 2956-2964 (2015).
- [13] Virmontois, C., Toulemont, A., Rolland, G., Materne, A., Lалуcaa, V., Goiffon, V., Codreanu, C., Durnez, C., and Bardoux, A., "Radiation-induced dose and single event effects in digital CMOS image sensors," *IEEE Trans. Nucl. Sci.* 61, 3331-3340 (2014).
- [14] McGrath, R. D., Doty, J., Lupino, G., Ricker, G., and Vallerga J., "Counting of Deep-Level Traps Using a Charge- Coupled Device," *IEEE Trans. Electron Devices* ED-34, 2555–2557 (1987).
- [15] Cohen, M., and David, J-P., "Radiation-induced dark current in CMOS active pixel sensors," *IEEE Trans. Nucl. Sci.* 47, 2485-2491 (2000).
- [16] Dale, C. J., Marshall, P. W., Burke, E. A., Summers, G. P., and Bender, G. E., "The generation lifetime damage factor and its variance in silicon," *IEEE Trans. Nucl. Sci.* 36, 1872-1881 (1989).
- [17] Srour, J. R., and Lo, D. H., "Universal damage factor for radiation-induced dark current in silicon devices," *IEEE Trans. Nucl. Sci.* 47, 2451-2459 (2000).
- [18] Srour, J. R., and Palko, J. W., "Displacement damage effects in irradiated semiconductor devices," *IEEE Trans. Nucl. Sci.* 60, 1740-1766 (2013).
- [19] EMVA Standard 1288 – Standard for characterization of image sensors and cameras, Release 3 (2010).
- [20] Beaumel, M., Herve, D., and Van Aken, D., "Cobalt-60, proton and electron irradiation of a radiation-hardened active pixel sensor," *IEEE Trans. Nucl. Sci.* 57, 2056-2065 (2010).